ACS APPLIED MATERIALS & INTERFACES

Research Article

www.acsami.org

Irradiation-Enhanced Reactivity of Multilayer Al/Ni Nanomaterials

Khachatur V. Manukyan,*[,†] Wanpeng Tan,[†] Richard J. deBoer,[†] Edward J. Stech,[†] Ani Aprahamian,[†] Michael Wiescher,[†] Sergei Rouvimov,[‡] Kyle R. Overdeep,[§] Christopher E. Shuck,[∥] Timothy P. Weihs,[§] and Alexander S. Mukasyan[∥]

[†]Nuclear Science Laboratory, Department of Physics, University of Notre Dame, Notre Dame, Indiana 46556, United States
[‡]Notre Dame Integrated Imaging Facility (NDIIF), University of Notre Dame, Notre Dame, Indiana 46556, United States
[§]Department of Materials Science and Engineering, Johns Hopkins University, Baltimore, Maryland 21218, United States
[∥]Department of Chemical and Biomolecular Engineering, University of Notre Dame, Notre Dame, Indiana 46556, United States

ABSTRACT: We have investigated the effect of accelerated ion beam irradiation on the structure and reactivity of multilayer sputter deposited Al/Ni nanomaterials. Carbon and aluminum ion beams with different charge states and intensities were used to irradiate the multilayer materials. The conditions for the irradiation-assisted self-ignition of the reactive materials and corresponding ignition thresholds for the beam intensities were determined. We discovered that relatively short (40 min or less) ion irradiations enhance the reactivity of the Al/Ni nanomaterials, that is, significantly decrease the thermal ignition temperatures (T_{ig}) and ignition delay times (τ_{ig}). We also show that irradiation leads to atomic mixing at the Al/Ni interfaces with the formation of an amorphous interlayer, in addition to the nucleation of small (2−3 nm) Al_3Ni crystals within the amorphous regions. The amorphous interlayer is thought to enhance the reactivity of the multilayer energetic nanomaterial by increasing the heat of the reaction and by speeding the intermixing of the Ni and the Al. The small Al_3Ni crystals may also enhance reactivity by facilitating the growth of this Al−Ni intermetallic phase. In contrast, longer irradiations decrease reactivity with higher ignition temperatures and longer ignition delay times. Such changes are also associated with growth of the Al_3Ni intermetallic and decreases in the heat of reaction. Drawing on this data set, we suggest that ion irradiation can be used to fine-tune the structure and reactivity of energetic nanomaterials.

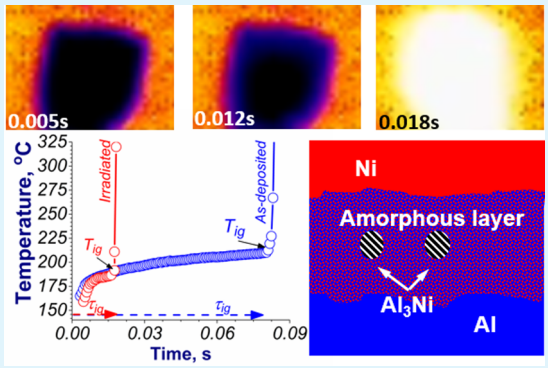

KEYWORDS: *energetic materials, nanostructured energetic composites, reactive multilayer foils, ion irradiation, ignition, self-propagating reaction*

1. INTRODUCTION

Nanostructured energetic composites are a class of materials that involve the combination of several high energy density, nonexplosive solids that undergo rapid energy release with tunable ignition sensitivity upon impact, friction, shock, electric spark, and/or thermal initiation.[1−15] There are different ways to prepare such materials. For example, recent studies[16−19] have shown that a number of nanostructured composites (Ni + Al, Ta + C, Ti + C) with high energy densities per volume can be prepared by high-energy ball milling. Magnetron sputtering and electron beam evaporation are also used to fabricate free-standing reactive multilayer nanostructured foils.[12,15,20−23] These techniques allow for fabrication of a wide range of nanostructured energetic composites because nearly all frequently used metals and metalloids can be deposited by choosing suitable deposition conditions. As-prepared, pore-free foils of reactive composites can be used in many applications, such as joining of materials,[24−27] in electronic devices,[28−30] initiation of secondary reactions,[31,32] preparation of nanostructured coatings,[33,34] etc.

One of the most extensively characterized reactive foils consists of nanoscale, alternating layers of Al and Ni.[35−43] The thickness of the individual layers varies between a few to hundreds of nanometers, while the total thicknesses of the foils typically range from 10 to 50 μm. Localized heating of Al/Ni foils by an electrical discharge or laser initiates a highly exothermic self-sustained reaction, which propagates in the form of a reaction wave along the foil with unusually high velocities (10−20 m/s). The reaction front temperatures increase from room temperature to 1500 °C in a microsecond time span. The ignition event is defined as the onset of a self-sustained chemical reaction and is commonly characterized by an *ignition temperature* (T_{ig}) and *ignition delay time* (τ) for a given heating rate.[44]

Characteristics of the self-propagating reaction (e.g., velocity of the reaction front, maximum combustion temperature) in reactive foils depend strongly on the average atomic diffusion

Received: February 12, 2015
Accepted: April 27, 2015
Published: April 27, 2015

DOI: 10.1021/acsami.5b01415
ACS Appl. Mater. Interfaces 2015, 7, 11272−11279

distance (bilayer spacing) of the reactants and the degree of intermixing at the layer interfaces.[35,45] The intermixing of reactants during deposition may reduce the reaction temperature because of the formation of solid solutions and/or metastable intermetallic phases. For relatively thick bilayers (>100 nm), intermixing has little effect. By decreasing the bilayer thickness below 20 nm though, the intermixed region becomes a larger fraction of the total volume, which results in the reduction of the reaction wave velocity.[35]

To understand the phase formation sequence in Al/Ni multilayer foils, different advanced methods such as calorimetry,[35,36,45,46] synchrotron time-resolved X-ray microdiffraction,[37,38] and dynamic transmission electron microscopy[47,48] were used. Calorimetry experiments with relatively low heating rates (1 °C/min) suggest that several exothermic steps exist between 200 and 700 °C that correspond to the formation of Al_9Ni_2, Al_3Ni, and Al_3Ni_2 intermediate phases and the AlNi final product.[35,36] However, in situ time-resolved X-ray microdiffraction[37,38] and dynamic electron microscopy[47,48] observations reveal that only the AlNi phase forms from a liquid Al−Ni solution during the self-propagating reaction. Heating rates in this case can reach well above 10^6 °C/s. Recently, atomic scale investigations[41−43] of the arrested reaction front also suggest that the aluminum first melts, followed by the partial dissolution of Ni into the melt,[43] where nucleation and growth of the AlNi phase takes place.

In the present work, we discover a novel approach to controlling the exothermic reactions in such reactive multilayer foils. Accelerated ion beams are used to tailor the reactivity of the Al/Ni foils by modifying the atomic structure at the layer interfaces. Specifically, we show that relatively short (40 min) high-energy (20 MeV) irradiation by $^{12}C^{4+}$ ions leads to a significant enhancement of reactivity, and we consider three possible sources for that enhancement: (i) a larger heat of mixing, (ii) more rapid interdiffusion due to the amorphous interlayers, and (iii) small Al_3Ni intermetallic nuclei that speed the growth of that intermetallic phase. In contrast, we also show that longer irradiation leads to a loss of reactivity.

2. EXPERIMENTAL SECTION

2.1. Material Fabrication. Multilayer Al/Ni foils were fabricated by direct current magnetron sputtering from Al (1100 alloy [99 wt % Al, 0.87 wt %, (Si,Fe) 0.12 wt % Cu]) and Ni (93 wt % Ni, 7 wt % V) targets at 800 and 500 W, respectively, onto polished brass substrates. Foils were deposited in 1 mTorr of argon (99.999% pure) in a vacuum chamber with a base pressure of less than 3×10^{-6} Torr. Vanadium was included in the nickel sputter target to make it nonmagnetic and thus allow for faster and more stable depositions. The relative thickness of Al and Ni layers was maintained at a 2.5:2 ratio leading to foils with an average stoichiometry of $Al_{44}Ni_{50}V_6$ with bilayer spacing of ∼65 nm and total thicknesses of ∼10 μm.

2.2. Ion Irradiation. Ion irradiation of the foils was performed using the FN Tandem Van de Graaff accelerator at the University of Notre Dame, Nuclear Science Laboratory. The Multi-Cathode Sputter Ion Source (SNICS) was used to generate continuous beams of carbon and aluminum charged particles. Irradiation of the foils was done at a normal incidence with $^{12}C^{4+}$ (20 MeV) and $^{27}Al^{6+}$ (50 MeV) ion beams, over a uniformly scanned irradiation diameter of 8 mm on the foils. The samples were held at room temperature. The ion beam current was maintained below 100 nA/cm^2 to avoid beam-heating of the samples. A K-type thermocouple probe, with wire thickness of 100 μm, was attached to foils to measure the temperature during irradiation. Such measurements showed that temperature of foils never exceeded 50 °C. Stopping and Range of Ions in Matter (SRIM)[49] calculations gave the projected ion range of ∼10 μm for both $^{12}C^{4+}$ and $^{27}Al^{6+}$ beams with stopping powers of 1.812 and 5.496 MeV/μm, respectively. SRIM calculations also showed that for both beams, approximately 99.9% of the ions pass through the foils and only 0.01% were trapped inside the foils. Samples were irradiated for varying durations, either 20, 40, 90, or 150 min.

2.3. Material Characterization. The phases in irradiated foils were determined by X-ray diffraction (XRD) analysis with Ni-filtered Cu−Kα radiation (D8 Advance, Bruker) operated at 40 kV and 40 mA. Step-scan data (of step size 0.025° and counting time 15 s) of foils were recorded over the angular range 20−90° (2θ). Atomic level structure analysis was performed with a Titan-300 (FEI) transmission electron microscope (TEM) with a resolution of 0.136 nm in scanning TEM (STEM) mode and about 0.1 nm information limit in high resolution TEM mode. The Titan is equipped with an energy dispersive X-ray spectroscopy (EDS, Oxford Inc.) system with a spectral energy resolution of 130 eV. The TEM samples were prepared using a Helios NanoLab 600 system by making cross-sectional slices from irradiated foils as described elsewhere.[43]

2.4. Reactivity Evaluation. A PerkinElmer DSC 8000 differential scanning calorimeter (DSC) was used to measure the heats of reaction of the initial and irradiated foils. In each DSC scan, ∼1−3 mg of foil was heated from 50 to 725 °C at a heating rate of 40 °C/min in flowing argon. The thermal ignition characteristics of foils, i.e., ignition temperature (T_{ig}) and delay time (τ_d), were obtained by using the method described elsewhere.[16]

Additionally, temperature profiles were obtained by cutting the foils into 2 × 2 mm pieces that were placed into a quartz tube that was preheated to 300 °C. The tube was 300 mm in length, 15 mm inner diameter, and 1 mm wall thickness, and the foils were inserted through a small opening (5 mm × 5 mm) in the middle of the tube. Pure argon (99.9998%) was purged (80 cm^3/min) through the tube for 10 min to eliminate air. A high-speed infrared camera (FLIR Systems, SC6000) positioned above the opening allowed measurement of the temperature−time history of the ignition process with a spatial resolution of 2 μm, temperature resolution of 5 °C, and recording speed of 2500 frames per second.

3. RESULTS

3.1. Irradiation of Foils. Two types of ion beams ($^{12}C^{4+}$ and $^{27}Al^{6+}$) with different intensities were used to irradiate the foils. It was shown that the minimum beam power sufficient to initiate a self-propagating reaction is higher for the $^{12}C^{4+}$ beam as compared to the $^{27}Al^{6+}$ beam. For example, the minimum power of an Al beam that initiates self-propagation in these samples is 0.25 W, while the ignition threshold for a carbon beam is much higher (0.42 W). Such a difference in ignition thresholds may be explained by different energies deposited in the Al/Ni foils. More detailed studies were carried out with the $^{12}C^{4+}$ beam as it is easier and more stable to produce then $^{27}Al^{6+}$.

A set of experiments with different exposure times with the $^{12}C^{4+}$ (0.4W) beam was performed to investigate the effect of irradiation on the phases and microstructure of the foils. The XRD patterns of the initial and irradiated foils are shown in Figure 1. It can be seen that the intensities of the diffraction peaks for the irradiated foils (curves b-d) decreased compared to the initial sample (curve a). The relative full width at half-maximum (fwhm) of the diffraction peaks for Al and Ni phases shows different trends depending on irradiation time. Figure 2 indicates that the relative fwhm of Ni (2 0 0) peak increases by ∼17% for 150 min of irradiation. Such a significant increase may be attributed to the decrease of the Ni crystallite size. In the case of the Al (1 1 1) peak, the relative fwhm increases by 2% (40 min), then decreases by 3.2% for an exposure time of 150 min. These results suggest that longer irradiation can facilitate the growth of Al crystallites.

DOI: 10.1021/acsami.5b01415
ACS Appl. Mater. Interfaces 2015, 7, 11272−11279

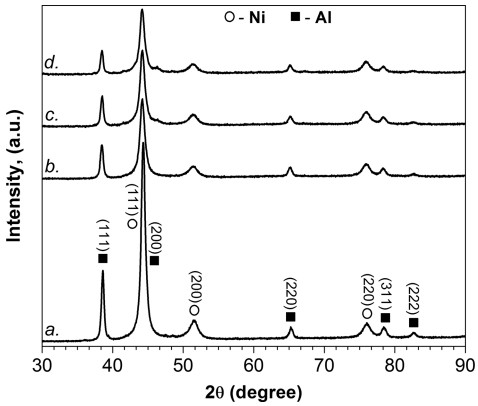

Figure 1. XRD patterns of the irradiated foils by the $^{12}C^{4+}$ beam with 0 (a), 40 (b), 90 (c), and 150 (d) minutes of irradiation.

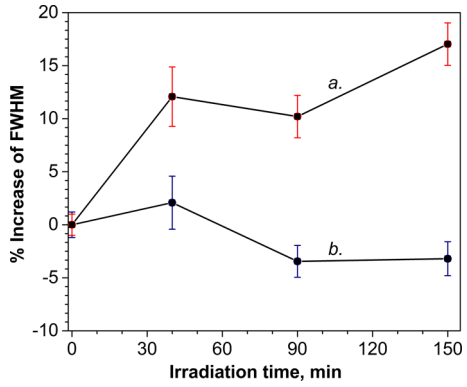

Figure 2. Relative full width at half maximums (fwhm) of Ni (200) (a) and Al (111) (b) peaks.

3.2. Microstructure of Foils. The cross-sectional bright field TEM images of the initial and beam exposed foils for 40 and 150 min are shown in Figure 3. The most pronounced structural transformations are the thinning of Ni layers (dark) and the thickening of Al layers (light) with more irradiation time. The results of electron diffraction pattern analysis (insets in Figure 3) with database values for *d*-spacings of Ni, Al and intermetallic phases are presented in Table 1. Evidently, the major phases present in the irradiated foils are Ni and Al. However, some new weak diffraction peaks that correspond to the Al_3Ni phase are present in the diffraction pattern of the irradiated foil for 40 min. After 150 min of beam exposure, many Al_3Ni phase diffraction lines are observed. The diffraction pattern of this foil also shows weak lines of the AlNi phase and several nonindexed lines, which may be related to the Al−Ni−V phases.

The cross-sectional STEM images (Figure 4A−C) also indicate that irradiation results in significant changes to the thicknesses of the Ni and Al layers. Figure 4A suggests that the thickness of the Ni layer in nonirradiated Al/Ni foil is ∼30 nm (see also Figure 4D). The Ni layer thicknesses for foils after 40 and 150 min of exposure are ∼28 (Figure 4B) and 22 nm (Figure 4C), respectively. These results are in good agreement with XRD data presented in Figures 1 and 2, suggesting that irradiation decreases the sizes of Ni crystallites. The opposite trend was observed for Al-rich layers. The thickness of Al layers in the initial foil is 35 nm (Figure 3A) and increases to 40 nm after 150 min of exposure.

STEM images (Figure 4B, C) also show that the irradiated foils have two distinct phases inside the Al-rich layer. Local EDS analysis reveals that the Al-rich layer in the 40 min irradiated foil contains, on average, 5 at.% of Ni. The Ni concentration in some brighter spots close to the layer interfaces can be as high as 25 at.%. These results suggest that the carbon beam facilitates solid-state diffusion of Ni into the Al layer. The contrast between the two distinct phases in the Al layer is enhanced in the foil that was irradiated for 150 min (Figure 4C). The large brighter grains contain 24 at.% Ni and 76 at.% Al. This finding, combined with the presence of Al_3Ni in the electron diffraction patterns (Figure 3B, Table 1), suggests that the large brighter grains are Al_3Ni.

The inner structure of the irradiated foil layers becomes more evident within the dark field TEM (Figure 5). Those images were obtained as dark field, and then underwent a negative transformation to obtain the conventional contrast of dark Ni and light Al phases. It can be seen that nuclei of Al_3Ni crystals are distributed in the Al-rich phase close to every other Al/Ni interface for the 40 min irradiated foil (Figure 5A). It is interesting that these nuclei line-up perpendicular to the direction of the incident beam (see Figure 5). Such structures confirm that the beam induces solid-state diffusion of Ni into the Al layer, where nucleation of the Al_3Ni phase takes place. Longer irradiation facilitates growth of the Al_3Ni nuclei to large grains inside the Al-rich layer that are clearly seen in Figure 5B and Figure 4C. Some of those Al_3Ni grains are large enough to cover the full Al-rich layer thickness.

The results of the high resolution TEM study of the atomic structure of the 40 min irradiated sample are summarized in Figure 6. Three different regions are marked at the Al/Ni interfaces (Figure 6A). Phases are identified based on direct

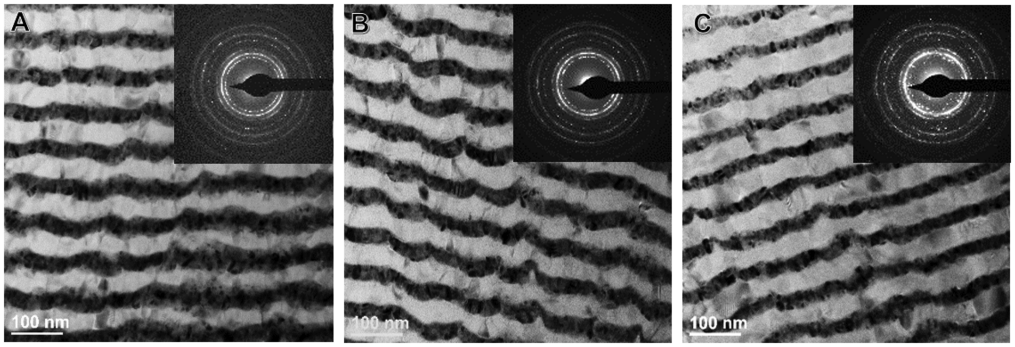

Figure 3. Cross-sectional bright-field TEM images of foils irradiated for 0 (A), 40 (B), and 150 (C) minutes: Ni and Al are the dark and white phases, respectively. Electron diffraction patterns are inserted.

DOI: 10.1021/acsami.5b01415
ACS Appl. Mater. Interfaces 2015, 7, 11272−11279

Table 1. Interpretation of the Electron Diffraction Patterns (inserts in Figure 3)

d-spacing, nm (measured)			*d*-spacing, nm (database)			
0 min	40 min	150 min	Ni	Al	Al_3Ni	AlNi
		0.428				
	0.384	0.383			0.389 (101)	
		0.364			0.368 (020)	
		0.287				0.286 (100)
	0.240	0.240			0.24 (220)	
2.325	0.2321	0.232		0.234 (100)		
		0.227			0.226 (102)	
		0.218			0.218 (031)	
		0.210			0.207 (131)	
0.203	0.202	0.203	0.203 (111)	0.202 (200)	0.201 (022)	0.203 (110)
	0.199	0.199			0.199 (301)	
	0.193	0.193			0.193 (311)	
		0.190			0.188 (212)	
0.177	0.177	0.176	0.176 (200)		0.176 (321)	
		0.151				
0.143	0.143	0.144		0.143 (220)		0.143 (200)
		0.140				
		0.129				0.128 (210)
0.125	0.125	0.125	0.125 (220)			
0.122	0.121			0.122 (311)		
0.117	0.117	0.114		0.117 (222)		
0.106	0.106	0.106	0.106 (311)			
0.102	0.103	0.101	0.102(311)			

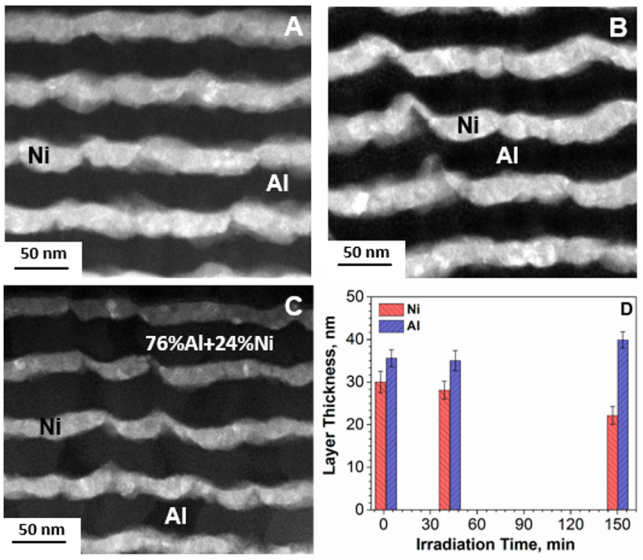

Figure 4. Scanning TEM images of the irradiated foils for 0 (A), 40 (B), and 150 (C) minutes, as well as measured thicknesses of Ni and Al layers (D).

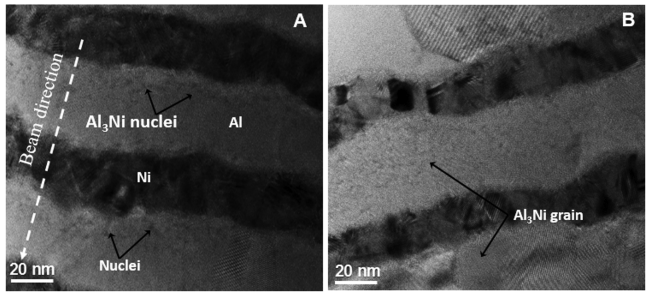

Figure 5. Bright field TEM images of the irradiated foils for 40 (A) and 150 (B) minutes.

measurements of *d*-spacing for highly crystalline Ni (Figure 6B) and defected Al (Figure 6C). An uneven amorphous interlayer with a thickness of ~10 nm can be seen in between crystalline phases (Figure 6D). The amorphous layer contains isolated nuclei of the Al_3Ni compound (interplanar spacing is 0.199 nm (3 0 1)) with average diameters of 2−3 nm.

3.3. Reactivity of Irradiated foils. Differential scanning calorimetry (DSC) with a heating rate of 40 °C/min is used to investigate the effect of ion irradiation on the heat of the reactions in layered Al/Ni nanomaterials (Figure 7A). Due to the nature of the irradiation process, only very small masses of each sample were available, but multiple scans were performed when possible. Therefore, the curve displayed for the initial foil (curve a) is the average of 3 runs; curves b and c were single runs, and curves (d) and (e) are averages of two runs.

The averaged DSC curve for the initial Al/Ni foils (curve a) exhibits three major exothermic peaks at 255, 320, and 425 °C. A small shoulder starting at 150 °C also exists prior to the first peak. This shoulder also can be seen on DSC curves for 20 min (curve b) and 40 min (curve c) irradiated foils. The onset temperature for the first exothermic peak for all irradiated foils is ~210 °C. The first peak of all beam-exposed foils has two reactions centered at ~230 and ~250 °C. While the temperature for the first reaction does not vary with irradiation time, the second reaction shifts down in temperature to approximately 248 °C with longer irradiation. Integration of each curve from 140 to 280 °C shows that irradiation for 20 or 40 min slightly increases the overall heat of the first peak (Figure 7B), but further irradiation up to 90 and 150 min causes the heat release to decrease. To approximate uncertainty in the measurements, the standard deviation found for the three nonirradiated samples is assumed for all irradiated samples.

DOI: 10.1021/acsami.5b01415
ACS Appl. Mater. Interfaces 2015, 7, 11272−11279

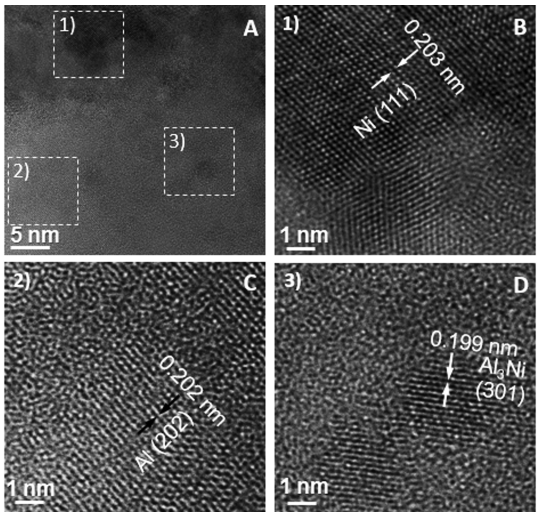

Figure 6. High resolution TEM images (A) of the Al/Ni interface of the irradiated foil for 40 min, magnified HRTEM images of nickel (B) and aluminum (C) layers, and amorphous interlayer with Al_3Ni nuclei (D).

The heat release for second and third peaks, occurring at 320 and 425 °C for the initial foils, do not seem to depend upon irradiation time, based on integrations performed from 280–334 and 334–460 °C. However, irradiation of the sample for 20 min causes the second and third peaks to shift to temperatures that are ~10 °C lower than the peak temperatures of the initial samples, but then continued irradiation up to 150 min causes temperatures for the second and third peaks to increase by ~5 °C.

High-speed infrared imaging is utilized to investigate the self-ignition characteristics of the foils, such as ignition temperature and delay time, as a function of irradiation time. The samples were uniformly heated on a heat source with a surface temperature of 300 °C and the temperature of the foils' surface was recorded. Time–temperature profiles (Figure 8) indicate that, upon contact with the heat source, the temperature of the foils increases rapidly from room temperature to about 180 °C with a heating rate of 4000 °C/s, which is 6×10^3 time faster than in the DSC experiments. Further heating is much slower with a rate of 300 °C/s, followed by an abrupt increase in heating rate (up to 2×10^5 °C/s) at some critical temperature, which here is defined as the ignition temperature (T_{ig}). The temperature profile (curve a) of nonirradiated foil shows that

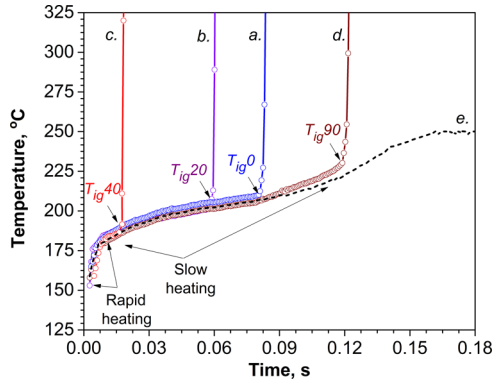

Figure 8. Temperature–time profiles of ignition for foils with 0 (a), 20 (b), 40 (c) 90 (d), and 150 (e) minutes of irradiation.

T_{ig} is 210 °C. T_{ig} for samples after 20 (curve b) and 40 (curve c) min of irradiation are lower than that for the initial foil. The sample with 90 min exposure time has a much higher T_{ig} (curve d). Finally, the sample irradiated for 150 min could not be ignited at the investigated conditions (curve e).

The values of T_{ig} and ignition delay time are summarized in Figure 9 as a function of irradiation time. Evidently, short-time

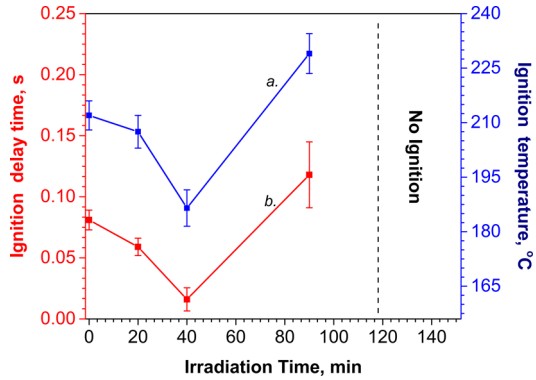

Figure 9. Ignition characteristics of the irradiated foils: ignition temperature (a) and ignition delay time (b).

beam exposure (40 min and below) is beneficial for increasing the reactivity of Al/Ni foils as ignition temperature drops from 210 to 180 °C (curve a). Ignition delay time (curve b) also decreases from 0.08 to 0.018 s. However, longer irradiation shows the opposite effect, that is, 90 min irradiated foils possess

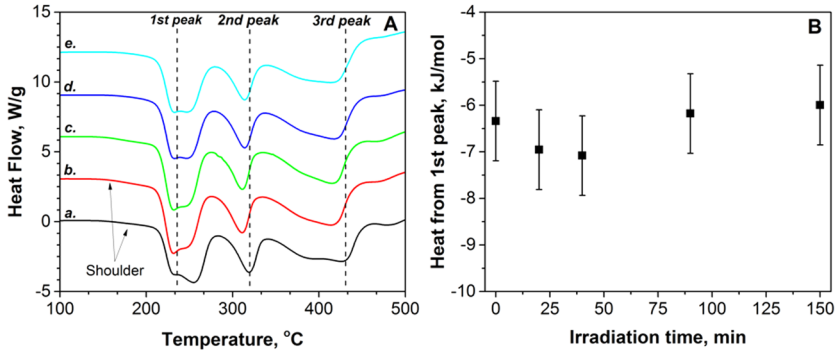

Figure 7. DSC curves (A) of the Al/Ni foils irradiated for 0 (a), 20 (b), 40 (c), 90 (d), and 150 (e) minutes, and the overall heat of the first peak as a function of irradiation time (B).

DOI: 10.1021/acsami.5b01415
ACS Appl. Mater. Interfaces 2015, 7, 11272–11279

higher ignition characteristics (Figure 9) compared to those for initial foils, and reactions cannot be ignited in the samples irradiated for 150 min.

4. DISCUSSION

High-energy ion irradiation of solids is well-known for damaging materials.[50] However, it has recently been demonstrated that it might have a beneficial effect in nanostructured materials. For example, the ion irradiation of layered nanostructures of metals results in their mixing and amorphization.[51−53] These processes are governed by collision cascades developed in elastic interactions of the impact ions with the atoms in the target material and the consequent secondary recoils; thermal spike mixing due to the heat generated locally around the ion tracks in inelastic interactions with electrons; and chemical reactivity of the constituents.[51,52] The latter can be dominant, enhancing mixing if the components are chemically reactive. Having a negative heat of mixing, the Al/Ni system belongs to a combination of materials that can mix readily. Thus, ion irradiation-induced mixing and formation of an amorphous interlayer in Al/Ni foils is enhanced by chemical driving forces.

Such amorphization is seen in the irradiated Al/Ni multilayers (Figure 6) and is shown schematically in Figure 10. We also note that Al_3Ni nanocrystals with sizes between

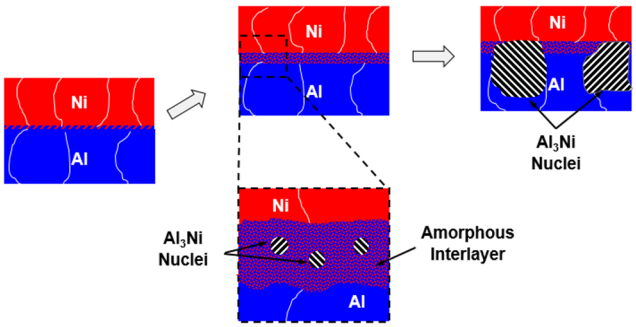

Figure 10. Schematic representation of ion irradiation modification of Al/Ni foils.

2−3 nm are observed within the amorphous regions after short irradiation times. Figure 5A shows that those nuclei are distributed at every other Al/Ni interface that was placed perpendicular to the incident beam. The mechanism of irradiation-induced crystallization of Al_3Ni is substantially different from previously described solid-state nucleation during the thermal annealing of foils,[54,55] where nuclei preferentially form at intergranular defects along the interface between two polycrystalline layers. After longer irradiation times, the Al_3Ni nanocrystals grow into larger crystals within the Al layers as shown via STEM in Figure 4C and schematically within Figure 10.

The ignition data in Figures 8 and 9 demonstrate that high-energy ion irradiation can enhance the reactivity of Al/Ni multilayered nanomaterials. Ignition temperatures and ignition delay times both decrease with 20 or 40 min of irradiation from a $^{12}C^{4+}$ beam, compared to those for the initial foils. An explanation for this effect lies in the modification of the nanolayer structure that is shown schematically in Figure 10. The initial Al/Ni foils are known to have a 2−3 nm intermixed crystalline layer at the interfaces between the two metals following deposition.[35] In Figures 3 to 6 we see that short-time (40 min or less) ion irradiation of these foils leads to additional mixing of the metals and the formation of an amorphous, alloyed interlayer with a thickness of 5−10 nm (see Figure 10). While the fast diffusion behavior of Ni in Al and the negative heat of mixing of Ni and Al suggest that this binary combination is a likely candidate for solid-state amorphization, such behavior has not been reported with slow or moderately fast heating of Al/Ni multilayer films or foils.[35,39,45] Thus, ion interaction with the Al and Ni layers is thought to be critical to the formation of the amorphous states. The question then arises, how these amorphous regions might enhance reactivity for bombardment times of 40 min or less.

Spontaneous crystallization of amorphous Al-rich layers is an *exothermic process* and could increase the total heat of reaction that drives the intermixing and phase formation. Using the heats of crystallization of pure Al (10.7 kJ/mol atom) and pure Ni (17.2 kJ/mol atom), we estimate a heat of crystallization of approximately 11.0 kJ/mol atom for the Al−5 at% Ni amorphous solutions. This raises the total heat of reaction, but the intermixing of Al and Ni that accompanies the amorphization lowers the total heat of reaction. Using the heat of mixing of Al and Ni in the liquid state we estimate a heat of mixing of 7 kJ/mol atom for the Al−5 at% Ni solution.[56] Combining the increase in the heat of reaction due to amorphization and the decrease in the heat of reaction due to intermixing, the net increase in the heat of reaction for the Al−5 at% Ni solution is 4 kJ/mol atom. While this estimate is slightly high due to the presence of some Al_3Ni nanocrystals in the amorphous phase, we can use it in conjunction with the atomic fraction of the amorphous phase to approximate a change in the heat released from the foils during the first exothermic peak (Figure 7B). If 20% of the Al atoms are amorphized following 40 min of irradiation, as is approximated based on volume fractions of each phase seen with HRTEM (Figure 6), then the amorphous Al−5 at% Ni phase represents approximately 9% of the atoms in the multilayer foil, and the heat measured for the first peak should increase by 0.4 kJ/mol atom. This estimate is smaller than, but quite close to, the increase in heat that is seen in Figure 7B for the first exotherm in the DSC curves. Consequently, we conclude that a higher thermodynamic driving force may be enhancing reactivity.

In addition to a higher driving force, two kinetic factors offer possible explanations as well. First, the amorphous Al−Ni phase should dramatically enhance the thermally induced intermixing that occurs during the self-ignition tests. Diffusion in amorphous phases is known to be much faster than in a chemically identical crystalline phase[57,58] and could lead to ignition at lower temperatures. Second, since the formation of intermetallic phases, such as Al_3Ni, are thought to occur in a two-stage process of nucleation and growth where nucleation can be the rate-limiting step,[59] a small volume fraction of Al_3Ni nuclei inside the amorphous interlayer could speed the growth of this phase and hence the ignition of the foils upon heating. Finally, the ignition data in Figures 8 and 9 also indicate that longer irradiation hinders the reaction kinetics, that is, leads to increasing T_{ig} and τ. In fact, after some critical exposure time the system cannot be ignited under current experimental conditions. This effect is attributed to more ion beam induced intermixing, substantial growth of Al_3Ni nuclei into large grains (Figures 4, 5, and 10), and a reduction in the thermodynamic driving force, based on a smaller heat release in the first exothermic peak. Thus, ion irradiation can also be used to "slow

DOI: 10.1021/acsami.5b01415
ACS Appl. Mater. Interfaces 2015, 7, 11272−11279

down" the reactions in high-energy density nanosystems, which could be beneficial for some applications.

We believe that ion irradiation is unique, when tuning the ignition properties of nanostructured energetic composites. While laser or thermal treatment can lead to intermixing in Al/Ni foils,[15,20] it will not induce amorphization. Without amorphization occurring during intermixing, the heat of reaction decreases and ignition temperature goes up. With ion irradiation both intermixing and amorphization can occur and under small doses ignition thresholds and temperatures can go down. Thus, ion irradiation is capable of both increasing and decreasing the reactivity and the kinetics of ignition in a controlled manner. Because of these advantages, it may become a general tool to tailor all possible reactive materials. No other technique is available to provide such a broad level of control over the structure and reactivity of reactive materials.

5. CONCLUSIONS

Using Al/Ni multilayer foils, we have shown that high-energy ion irradiation with a $^{12}C^{4+}$ beam can be an effective tool for tailoring the chemical reactivity of nanostructured materials. Short irradiation times lead to lower ignition temperatures, shorter ignition delay times, slightly larger heats of reaction, and an increase in reactivity for the foils, while long exposures increase ignition temperatures and delay times, as well as lower heats of reaction and reactivity. Both sets of changes are associated with atomic level modifications of the Al/Ni interfaces. The formation of an amorphous Al−Ni alloy during short irradiations is shown to raise the heat released in DSC scans, and thus is thought to increase the driving force for the overall reaction. The amorphous phase may also speed thermally driven Al−Ni intermixing during ignition, compared to as-deposited foils. In a similar manner, the presence of Al_3Ni nanocrystals could speed growth of the intermetallic. Both kinetic factors could enhance reactivity. After longer irradiation times, though, heat released in the DSC scans decreases as the Al_3Ni crystals have grown at the expense of the amorphous phase and reactivity decreases. Future work should explore whether such high-energy ion irradiation can be used to tune the microstructure and reactivity of other nanoscaled reactive systems.

AUTHOR INFORMATION

Corresponding Author

*Phone: +1-574-631-6083. E-mail: kmanukya@nd.edu.

Notes

The authors declare no competing financial interest.

ACKNOWLEDGMENTS

This work is supported by the National Science Foundation, under Grant No. PHY-1419765. T.P.W. was supported by National Science Foundation (NSF) Grant DMR-1308966, and K.R.O was supported by DTRA Grant HDTRAA1-11-1-0063. A.S.M. was supported by DTRA grant HDTRA1-10-1-0119, and C.E.S. was supported by National Nuclear Security Administration Grant DE-NA0002377.

REFERENCES

(1) Zhou, X.; Torabi, M.; Lu, J.; Shen, R.; Zhang, K. Nanostructured Energetic Composites: Synthesis, Ignition/Combustion Modeling, and Applications. *ACS Appl. Mater. Interfaces* **2014**, *6*, 3058−3074.

(2) Dreizin, E. L. Metal-Based Reactive Nanomaterials. *Prog. Energy Combust. Sci.* **2009**, *35*, 141−167.

(3) Rossi, C.; Zhang, K.; Esteve, D.; Alphonse, P.; Philippe, T.; Vahlas, C. Nanoenergetic Materials for MEMS: A Review. *J. Microelectromech. Syst.* **2007**, *16*, 919−931.

(4) Rogachev, A. S.; Mukasyan, A. S. Combustion of Heterogeneous Nanostructural Systems (Review). *Combust. Explos. Shock Waves* **2010**, *46*, 243−266.

(5) Yetter, R. A.; Risha, G. A.; Son, S. F. Metal Particle Combustion and Nanotechnology. *Proc. Combust. Inst.* **2009**, *32*, 1819−1838.

(6) Feng, J.; Jian, G.; Liu, Q.; Zachariah, M. R. Passivated Iodine Pentoxide Oxidizer for Potential Biocidal Nanoenergetic Applications. *ACS Appl. Mater. Interfaces* **2013**, *5*, 8875−8880.

(7) Sabourin, J. L.; Dabbs, D. M.; Yetter, R. A.; Dryer, F. L.; Aksay, I. A. Functionalized Graphene Sheet Colloids for Enhanced Fuel/Propellant Combustion. *ACS Nano* **2009**, *3*, 3945−3954.

(8) Kwon, J.; Ducéré, J.; Alphonse, P.; Bahrami, M.; Petrantoni, M.; Veyan, J.-F.; Christophe, T.; Alain, E.; Rossi, C.; Chabal, Y. J. Interfacial Chemistry in Al/CuO Reactive Nanomaterial and Its Role in Exothermic Reaction. *ACS Appl. Mater. Interfaces* **2013**, *5*, 605−613.

(9) Martirosyan, K. S. Nanoenergetic Gas-Generators: Principles and Applications. *J. Mater. Chem.* **2011**, *21*, 9400−9405.

(10) Slocik, J. M.; Crouse, C. A.; Spowart, J. E.; Naik, R. R. Biologically Tunable Reactivity of Energetic Nanomaterials Using Protein Cages. *Nano Lett.* **2013**, *13*, 2535−2540.

(11) Dong, Z.; Al-Sharab, J. F.; Kear, B. H.; Tse, S. D. Combined Flame and Electrodeposition Synthesis of Energetic Coaxial Tungsten-Oxide/Aluminum Nanowire Arrays. *Nano Lett.* **2013**, *13*, 4346−4350.

(12) Adams, D. P. Reactive Multilayers Fabricated by Vapor Deposition: A Critical Review. *Thin Solid Films* **2015**, *576*, 98−128.

(13) Wei, C. T.; Nesterenko, V. F.; Weihs, T. P.; Remington, B. A.; Park, H.-S.; Meyers, M. A. Response of Ni/Al Laminates to Laser-Driven Compression. *Acta Mater.* **2012**, *60*, 3929−3942.

(14) Blobaum, K. J.; Reiss, M. E.; Plitzko, J. M.; Weihs, T. P. Deposition and Characterization of a Self-propagating CuO_x/Al Thermite Reaction in a Multilayer Foil Geometry. *J. Appl. Phys.* **2003**, *94*, 29152−292922.

(15) Weihs, T. P. Fabrication and Characterization of Reactive Multilayer Films and Foils. In *Metallic Films for Electronic, Magnetic, Optical and Thermal Applications: Structure, Processing and Properties*; Barmak, K., Coffey, K. R., Eds.; Woodhead Publishing, Swaston, U.K., 2014; Chapter 6, 160−243.

(16) Manukyan, K. V.; Lin, Y.-C.; Rouvimov, S.; McGinn, P. J.; Mukasyan, A. S. Microstructure-Reactivity Relationship of Ti + C Reactive Nanomaterials. *J. Appl. Phys.* **2013**, *113*, No. 024302.

(17) Manukyan, K. V.; Mason, B. A.; Groven, L. J.; Lin, Y.-C.; Cherukara, M.; Son, S. F.; Strachan, A.; Mukasyan, A. S. Tailored Reactivity of Ni + Al Nanocomposites: Microstructural Correlations. *J. Phys. Chem. C* **2012**, *116*, 21027−21038.

(18) Bacciochini, A.; Bourdon-Lafleur, S.; Poupart, C.; Radulescu, M.; Jodoin, B. Ni−Al Nanoscale Energetic Materials: Phenomena Involved During the Manufacturing of Bulk Samples by Cold Spray. *J. Therm. Spray Technol.* **2014**, *23*, 1142−1148.

(19) Shteinberg, A. S.; Lin, Y.-C.; Son, S. F.; Mukasyan, A. S. Kinetics of High Temperature Reaction in Ni−Al System: Influence of Mechanical Activation. *J. Phys. Chem. A* **2010**, *114*, 6111−6116.

(20) Fritz, G. M.; Spey, S. J.; Grapes, M. D.; Weihs, T. P. Thresholds for Igniting Exothermic Reactions in Al/Ni Multilayers using Pulses of Electrical, Mechanical, and Thermal Energy. *J. Appl. Phys.* **2013**, *113*, No. 014901.

(21) Reiss, M. E.; Esber, C. M.; Van Heerden, D.; Gavens, A. J.; Williams, M. E.; Weihs, T. P. Self-propagating Formation Reactions in Nb/Si Multilayers. *Mater. Sci. Eng., A* **1999**, *261*, 217−222.

(22) Reeves, R. V.; Adams, D. P. Reaction Instabilities in Co/Al Nanolaminates Due to Chemical Kinetics Variation over Micron-Scales. *J. Appl. Phys.* **2014**, *115*, No. 044911.

(23) Rogachev, A. S. Exothermic Reaction Waves in Multilayer Nanofilms. *Russ. Chem. Rev.* **2008**, *77*, 21−37.

(24) Wang, J.; Besnoin, E.; Duckham, A.; Spey, S. J.; Reiss, M. E.; Knio, O. M.; Powers, M.; Whitener, M.; Weihs, T. P. Room-

DOI: 10.1021/acsami.5b01415
ACS Appl. Mater. Interfaces 2015, 7, 11272−11279

Temperature Soldering with Nanostructured Foils. *Appl. Phys. Lett.* **2003**, *83*, 3987−3989.
(25) Duckham, A.; Spey, S. J.; Wang, J.; Reiss, M. E.; Weihs, T. P.; Besnoin, E.; Knio, O. M. Reactive Nanostructured Foil used as a Heat Source for Joining Titanium. *J. Appl. Phys.* **2004**, *96*, 2336−2342.
(26) Wang, J.; Besnoin, E.; Duckham, A.; Spey, S. J.; Reiss, M. E.; Knio, O. M.; Weihs, T. P. Joining of Stainless-Steel Specimens with Nanostructured Al/Ni foils. *J. Appl. Phys.* **2004**, *95*, 248−256.
(27) Swiston, A. J.; Hufnagel, T. C.; Weihs, T. P. Joining Bulk Metallic Glass using Reactive Multilayer Foils. *Scr. Mater.* **2003**, *48*, 1575−1580.
(28) Braeuer, J.; Besser, J.; Wiemer, M.; Gessner, T. A Novel Technique for MEMS Packaging: Reactive Bonding with Integrated Material Systems. *Sens. Actuators, A* **2012**, *188*, 212−219.
(29) Qiu, X.; Wang, J. Bonding Silicon Wafers with Reactive Multilayer Foils. *Sens. Actuators. A* **2008**, *141*, 476−481.
(30) Boettge, B.; Braeuer, J.; Wiemer, M.; Petzold, M.; Bagdahn, J.; Gessner, T. J. Fabrication and Characterization of Reactive Nanoscale Multilayer Systems for Low-temperature Bonding in Microsystem Technology. *J. Micromech. Microeng.* **2010**, *20*, No. 064018.
(31) Morris, C. J.; Wilkins, P.; May, C.; Zakar, E.; Weihs, T. P. Streak Spectrograph Temperature Analysis from Electrically Exploded Ni/Al Nanolaminates. *Thin Solid Films* **2011**, *520*, 1645−1650.
(32) Qiu, X.; Tang, R.; Liu, R.; Huang, H.; Guo, S.; Yu, H. A Micro Initiator Realized by Reactive Ni/Al Nanolaminates. *J. Mater. Sci. Mater. Electron.* **2012**, *23*, 2140−2144.
(33) Ramos, A. S.; Vieira, M. T.; Morgiel, J.; Grzonka, J.; Simões, S.; Vieira, M. F. Production of Intermetallic Compounds from Ti/Al and Ni/Al Multilayer Thin Films—A Comparative Study. *J. Alloys Compd.* **2009**, *484*, 335−340.
(34) McDonald, J. P.; Rodriguez, M. A.; Jones, E. D.; Adams, D. P. Rare-Earth Transition-Metal Intermetallic Compounds Produced via Self-Propagating, High-Temperature Synthesis. *J. Mater. Res.* **2011**, *25*, 718−727.
(35) Gavens, A. J.; Van Heerden, D.; Mann, A. B.; Reiss, M. E.; Weihs, T. P. Effect of Intermixing on Self-Propagating Exothermic Reactions in Al/Ni Nanolaminate Foils. *J. Appl. Phys.* **2000**, *87*, 1255−1263.
(36) Blobaum, K. J.; Van Heerden, D.; Gavens, A. J.; Weihs, T. P. Al/Ni Formation Reactions: Characterization of the Metastable Al_9Ni_2 Phase and Analysis of its Formation. *Acta Mater.* **2003**, *51*, 3871−3884.
(37) Trenkle, J. C.; Koerner, L. J.; Tate, M. W.; Gruner, S. M.; Weihs, T. P.; Hufnagel, T. C. Phase Transformations During Rapid Heating of Al/Ni Multilayer Foils. *Appl. Phys. Lett.* **2008**, *93*, 081903 1−3.
(38) Trenkle, J. C.; Koerner, L. J.; Tate, M. W.; Walker, N.; Gruner, S. M.; Weihs, T. P.; Hufnagel, T. C. Time-Resolved X-ray Microdiffraction Studies of Phase Transformations During Rapidly Propagating Reactions in Al/Ni and Zr/Ni Multilayer Foils. *J. Appl. Phys.* **2010**, *107*, No. 113511.
(39) Grapes, M. D.; LaGrange, T.; Woll, K.; Reed, B. W.; Campbell, G. H.; LaVan, D. A.; Weihs, T. P. In Situ Transmission Electron Microscopy Investigation of the Interfacial Reaction between Ni and Al during Rapid Heating in a Nanocalorimeter. *APL Mater.* **2014**, *2*, No. 116102.
(40) Swaminathan, P.; Grapes, M. D.; Woll, K.; Barron, S. C.; LaVan, D. A.; Weihs, T. P. Studying Exothermic Reactions in the Ni−Al system at Rapid Heating Rates using a Nanocalorimeter. *J. Appl. Phys.* **2013**, *113*, 143509 1−8.
(41) Rogachev, A. S.; Vadchenko, S. G.; Mukasyan, A. S. Self-Sustained Waves of Exothermic Dissolution in Reactive Multilayer Nano-foils. *Appl. Phys. Lett.* **2012**, *101*, No. 063119.
(42) Politano, O.; Baras, F.; Mukasyan, A. S.; Vadchenko, S. G.; Rogachev, A. S. Microstructure Development During NiAl Intermetallic Synthesis in Reactive Ni−Al Nanolayers: Numerical Investigations vs. TEM Observations. *Surf. Coat. Technol.* **2013**, *215*, 485−492.
(43) Rogachev, A. S.; Vadchenko, S. G.; Baras, F.; Politano, O.; Rouvimov, S.; Sachkova, N. V.; Mukasyan, A. S. Structure Evolution and Reaction Mechanism in the Ni/Al Reactive Multilayer Nanofoils. *Acta Mater.* **2014**, *66*, 86−96.
(44) Frank-Kamenetskii, D. *Diffusion and Heat Exchange in Chemical Kinetics*; Princeton University Press: Princeton, NJ, 1955.
(45) Knepper, R.; Snyder, M. R.; Fritz, G.; Fisher, K.; Knio, O. M.; Weihs, T. P. Effect of Varying Bilayer Spacing Distribution on Reaction Heat and Velocity in Reactive Al/Ni Multilayers. *J. Appl. Phys.* **2009**, *105*, No. 083504.
(46) Nathani, H.; Wang, J.; Weihs, T. P. Long-Term Stability of Nanostructured Systems with Negative Heats of Mixing. *J. Appl. Phys.* **2007**, *101*, No. 104315.
(47) Kim, J.; LaGrange, T.; Reed, B.; Taheri, M. L.; Armstrong, M. R.; King, W. E.; Browning, N. D.; Campbell, G. H. Imaging of Transient Structures Using Nanosecond in Situ TEM. *Science* **2008**, *321*, 1472−1476.
(48) Kim, J. S.; LaGrange, T.; Reed, B. W.; Knepper, R.; Weihs, T. P.; Browning, N. D.; Campbell, G. H. Direct Characterization of Phase Transformations and Morphologies in Moving Reaction Zones in Al/Ni Nanolaminates Using Dynamic Transmission Electron Microscopy. *Acta Mater.* **2011**, *59*, 3571−3580.
(49) Ziegler, J. F.; Biersack, J. P.; Littmark, U. *The Stopping and Range of Ions in Solids*; Pergamon: New York, 1985; http://www.srim.org.
(50) Krasheninnikov, A. V.; Nordlund, K. Ion and Electron Irradiation-induced Effects in Nanostructured Materials. *J. Appl. Phys.* **2010**, *107*, No. 071301.
(51) Liu, B. X.; Lai, W. S.; Zhang, Q. Irradiation Induced Amorphization in Metallic Multilayers and Calculation of Glass-Forming Ability from Atomistic Potential in the Binary Metal Systems. *Mater. Sci. Eng., R.* **2000**, *29*, 1−48.
(52) Milosavljević, M.; Toprek, D.; Obradović, M.; Grce, A.; Peruško, D.; Dražič, G.; Kovač, J.; Homewood, K. P. Ion Irradiation Induced Solid-state Amorphous Reaction in Ni/Ti Multilayers. *Appl. Surf. Sci.* **2013**, *268*, 516−523.
(53) Zhao, B.; Yang, G. H.; Zeng, F.; Pan, F. Irradiation Induced Alloying and Formation of Amorphous Films in Co−Mo System During Ion Beam Assisted Deposition. *Acta Mater.* **2003**, *51*, 5093−5099.
(54) Ma, E.; Thompson, C. V.; Clevenger, L. A. Nucleation and Growth During Reactions in Multilayer Al/Ni Films: The Early Stage of Al_3Ni Formation. *J. Appl. Phys.* **1991**, *69*, 2211−2218.
(55) Ma, E.; Clevenger, L. A.; Thompson, C. V. Nucleation of an Intermetallic at Thin-Film Interfaces: VSi_2 Contrasted with Al_3Ni. *J. Mater. Res.* **1992**, *7*, 1350−1355.
(56) Stolz, U. K.; Arpshofen, I.; Sommer, F.; Predel, B. Determination of the Enthalpy of Mixing of Liquid Alloys Using a High-Temperature Mixing Calorimeter. *J. Phase Equilib.* **1993**, *14*, 473−478.
(57) Schwarz, R. B.; Johnson, W. L. Formation of an Amorphous Alloy by Solid-State Reaction of the Pure Polycrystalline Metals. *Phys. Rev. Lett.* **1983**, *51*, 415−418.
(58) Holloway, K.; Sinclair, R. Amorphous Ti−Si Alloy Formed by Interdiffusion of Amorphous Si and Crystalline Ti Multilayers. *J. Appl. Phys.* **1987**, *61*, 1359−1364.
(59) Fine, M. E. *Introduction to Phase Transformations in Condensed Systems*; Macmillan: London, 1964.

DOI: 10.1021/acsami.5b01415
ACS Appl. Mater. Interfaces 2015, 7, 11272−11279